DOI: https://doi.org/10.38027/ICCAUA2024EN0242

New Anchorage Technique for GFRP Flexural Strengthening of Concrete Beams Using Bolts-End Anchoring System

* [1] Assoc. Prof. Dr. **Djarir Yahiaoui,** [2] Prof. Dr. **Mohamed Saadi**, [1]
[1 &2] *LGC-ROI, Civil Engineering Laboratory-Risks and Structures in Interactions, Department of Civil Engineering, Faculty of Technology, University of Batna 2, 05001 Batna, Algeria*
E-mail [1]: d.yahiaoui@univ-batna2.

Abstract
The concept of external glass FRP composite confinement is a current process for strengthening concrete beams subjected to static loads. End anchorage glass FRP composites of 80 mm width and 90–130 mm length with different thicknesses (2.4 and 4.8 mm) have been fixed at the bottom of beams with bolts of various diameters (6 and 10 mm). It is concluded that the load capacity of the BEGFPC beams is improved by increasing the end-anchorage glass FRP composite thickness (about 98–188%). In addition, the BEGFPC system with bolts of 6 mm diameter has significantly improved the flexibility of beams. In contrast, the 10 mm bolts in diameter give a high ultimate load, whatever their quantity. Therefore, combining bolts with diameters of 6 and 10 mm would be the best solution for increasing the ultimate load and ductility of the retrofitted beams.
Keywords: Tension zone; Bolts-end anchoring; Glass FRP; Bolts; Crack patterns Failure modes.

1. Introduction

Strengthening and rehabilitating degraded concrete structures by external bonding is a fruitful technique. Steel plates are popular due to their high strength, flexibility, and homogenous characteristics (Alasadi et al., 2019). However, steel plates corrode and lose thickness if exposed to open environments. Significantly, the influence of corrosion is limited by covering the concrete parts with anti-corrosive compounds, such as carbon fiber reinforced polymer (CFRP), glass FRP, aramid FRP, and basalt FRP (Al-Hamrani & Alnahhal, 2019; Norooz Olyaee & Mostofinejad, 2019; Yahiaoui et al., 2022). These FRPs are available in rebar, laminate, or sheet form. More importantly, the FRPs are lightweight, strong, and more cost-effective components to manufacture than metal plates. Therefore, the external FRPs bonding process has been widely used to strengthen concrete beams, because it makes the material more ductile (El Ghadioui et al., 2022; Pavithra et al., 2022). Prior studies reported that the FRP composites remained elastic until brittle debonding or FRP failure occurred (Salama et al., 2019; Zhou et al., 2018). The effects of fiber direction and reinforcement ratio of glass fiber reinforced polymer (GFRP) sheets have been analyzed to examine the behavior of concrete beams. It is reported that the GFRP sheets strengthen the beam and improve the flexural deflection of the beams (Sankaramoorthy et al., 2022). Furthermore, many researchers recommended using hybrid FRP composites, including diverse kinds of fiber sheets, to enhance the efficiency of such strengthening processes. This design would cause the failure to occur at different strains of the sheets under loading, allowing the composites to fail gradually and thereby enhancing the flexibility of the strengthened element (Vahidpour et al., 2022). Various flexural tests have been performed on hybrid CFRP/ GFRP-concrete beams with CFRP layers in flanges. The optimal volume percentage of carbon fiber was determined to be 25–33% (Nguyen et al., 2015). Additional research conducted an experimental assessment of strengthened concrete beams by various combinations, including carbon-glass fabric and vegetable fiber. It is revealed that all reinforced beams provide superior characteristics to the controlled beam, with significant bending loading improvements (Djeddi et al., 2016).
Therefore, this work proposes a performed design process for the flexural behavior of beams with bolt-end anchoring glass fiber polymer composites (BEGFPC). Furthermore, the present study evaluates the effect of the BEGFRPC layer thickness, bolts diameter, and its arrangement on the flexural performance and bonding behavior of concrete beams externally strengthening under threepoint loading. Twenty-two beams are divided into three series and were tested. The beam control is strengthened only in flexure with a GFRP sheet of 2.4 mm thickness. The second series of beams are reinforced with a GFRP sheet and bolts. The third series of beams is strengthened with a GFRP sheet and bolts-end anchoring GFRP with different thicknesses (2.4 and 4.8 mm). The experimental results incorporate load versus mid-span deflection response curve, elastic stiffness, ultimate loads and flexural capacity, energy absorption capacity, and associated failure mode of the tested beams.

2 Experimental Program

This section presents the different materials' mechanical properties, the test setup description, and the procedures used to investigate the bond properties.

2.1 Materials

2.1.1 Concrete

The concrete mix is prepared with Ordinary Portland cement. The mixture is designed to reach an average compressive strength of 25–30 MPa at 28 days. It is elaborated using a water/cement ratio of 0.57, according to the ACI-211.1-91 design procedure (ACI211.1, 2009). The effect of fine and coarse aggregates has been considered, as reported by (Nili et al., 2017). The mix is cast into (150×150×150 mm) molds for compression testing. Then, the samples are tested after 28 days to measure compressive strength according to (ASTM C39/C39M- 17b, 2017). The average compressive strength after 28 days is 25 MPa, Table 1.

2.1.2 Glass Fiber Reinforced Polymer

Local polyester resin and bidirectional fiber-glass are used to develop a low-cost glass fiber-reinforced polymer composite, as shown in Fig. 1.

In the boating industry, this category of bi-directional fiber-glass is commonly used. For strengthening GFRC beams, glass FRP composites were prepared and tested using the UTS-SHIMADZU universal machine according to the standard guidelines of (ASTM D638-10, 2010). Three tensile samples of FRP Composite were tested to obtain accurate results, as shown in Table 2;

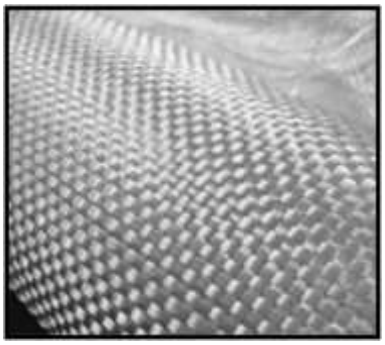

Fig. 1 Bi-directional glass fiber reinforced polymer (GFRP).

Table 1 Mix proportion of the C25 concrete

Material	Cement (kg/m³)	Sand (kg/m³)	Coarse aggregate (kg/m³)	Fine aggregate (kg/m³)	Water (kg/m³)	Superplasticizer (% cement weight)	Compressive Strength (MPa)
	400	773	496	496	163	0.9–1.1	25

Table 2 Mechanical properties of epoxy resin and GFRP composite

FRP Composite	Tensile stress (MPa)	Ultimate strain (%)	Modulus of elasticity (GPa)	Standard deviation
Epoxy resin	17.20	0.6322	2.72	1.08
GFRP	377.64	2.04%	43	1.91

2.2 Specimen and Anchoring System

As mentioned, the mixture is cast into (500×150×150 mm) molds for three-point testing. First, the beam specimens are demolded after 24 h from casting and left in a controlled environment at a temperature of 20 °C and relative humidity of 100% for 28 days. Then, the polyester resin is applied to the sample's external surface with a brush. Then, a resin-soaked fiberglass board is covered at the bottom of the concrete beam. The concrete surface is adequately cleaned to remove dust before applying the GFRP compound. The last strengthened specimen is shown in Fig. 2a. To increase the bonding between the GFRP sheets and the concrete beam, the GFRP anchor plates are connected to the bottom by bolts, as shown in Fig. 2c, b. In addition, the reason for using anchoring plates with different thicknesses at the bottom of the beam is to distribute the stresses generated from the bolts on the concrete surface. The dimensions and location of holes for the plates (1, 2, 3, 4, and 5) are shown in Fig. 2d. Moreover, the diameters of the bolts are 6 and 10 mm. The beams' designations summary and the parameters of investigation are presented in Table 3 and Fig. 3.

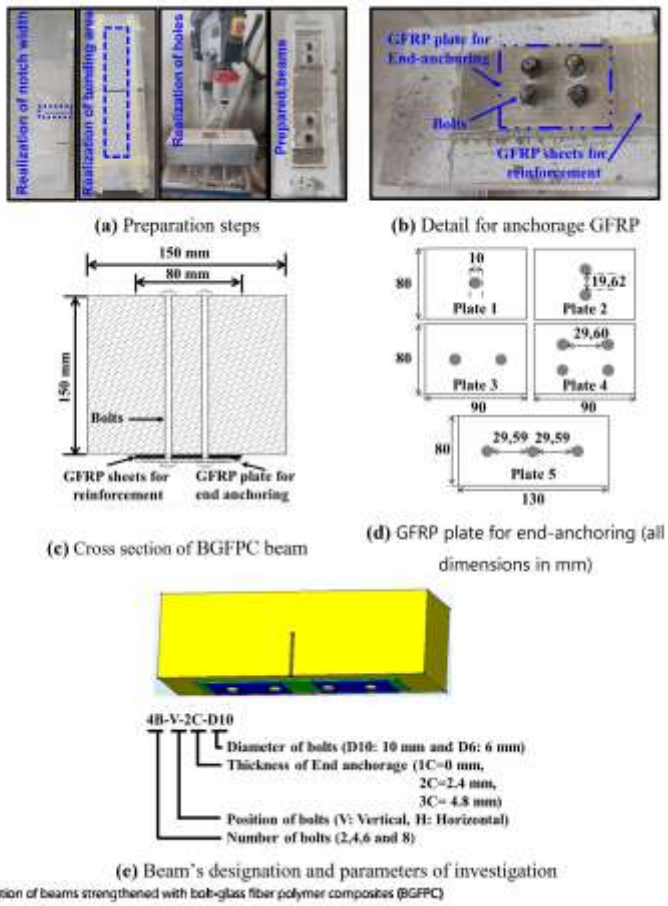

(a) Preparation steps (b) Detail for anchorage GFRP

(c) Cross section of BGFPC beam (d) GFRP plate for end-anchoring (all dimensions in mm)

(e) Beam's designation and parameters of investigation

Fig. 2 Preparation of beams strengthened with bolt-glass fiber polymer composites (BGFPC)

Table 3 Technical details of the end-anchorages and the bolts

Specimen	End anchorage	Thickness of end-anchorage (mm)	Number of bolts	Position of bolts	Bolt diameter (mm)
B0-1C	Without	0	0	-	0
B2-1C-D10	Without	0	2	-	10
B4-H-1C-D10	Without	0	4	Horizontal	10
B4-H-1C-D6	Without	0	4	Horizontal	6
B4-V-1C-D10	Without	0	4	Vertical	10
B6-V-1C-D10	Without	0	6	Vertical	10
B8-H-1C-D10	Without	0	8	Horizontal	10
B8-H-1C-D6	Without	0	8	Horizontal	6
B2-2C-D10	With	2.4	2	Horizontal	10
B4-H-2C-D10	With	2.4	4	Horizontal	10
B4-H-2C-D6	With	2.4	4	Horizontal	6
B4-V-2C-D10	With	2.4	4	Vertical	10
B6-V-2C-D10	With	2.4	6	Vertical	10
B8-H-2C-D10	With	2.4	8	Horizontal	10
B8-H-2C-D6	With	2.4	8	Horizontal	6
B2-3C-D10	With	2.4	2	-	10
B4-H-3C-D10	With	4.8	4	Horizontal	10
B4-H-3C-D6	With	4.8	4	Horizontal	6
B4-V-3C-D10	With	4.8	4	Vertical	10
B6-V-3C-D10	With	4.8	6	Vertical	10
B8-H-3C-D10	With	4.8	8	Horizontal	10
B8-H-3C-D6	With	4.8	8	Horizontal	6

2.3 Test Setup

According to (ASTM D7958/D7958M, 2017), three-point bending tests are performed, as shown in Fig. 3. The tests are conducted through universal test equipment with a load capacity of 200 kN. Quasi-static loading is a process in which the vertical displacement of the beam change infinitely slowly; thus, the system appears nearly static. It is an ideal process that is reversible and experiences equilibrium at every test stage. Therefore, the displacement rate is controlled at 0.05 mm/min for GFRP-strengthened beams. The load is registered during the entire test with the integrated load sensor of the test equipment. At the same time, the deflection of the control point is monitored using a linear variable displacement transducer (LVDT) which is rigidly attached to the roller usedfor the load application. The tests were stopped when the load applied after achieving the peak load was about 20% of the ultimate load.

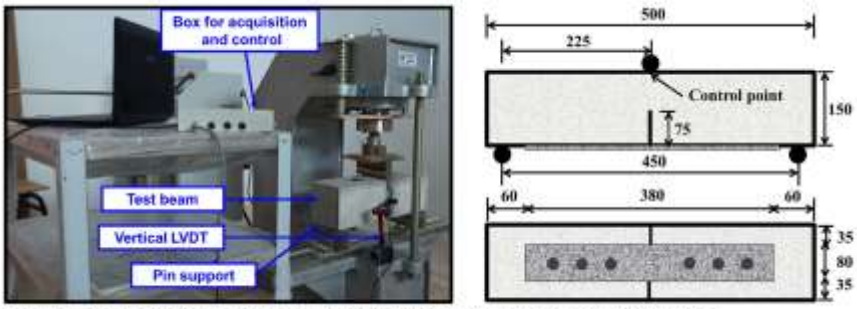

Fig. 3 Loading device and specimen dimension according to ASTM D7958/D7958M regulation (all dimensions in mm)

3 Experimental Results

3.1 Load–Deflection Relationship

The load versus deflection results are shown in Figs. 4, 5 and 6 for all beams. The curves are used to assess the effect of the end-anchorage GFRP thickness, the number, the position, and the diameter of the bolts. Compared with specimen 0B-1C, a more extended elastic stage and a higher stiffness are presented with the inclusion of the end-anchorage system GFRP. The typical load–deflection relationships are divided into three types of curves.

Initially, the first type is described in specimen 0B-1C. When the load increases linearly up to 23 kN, it drops sharply, because the interface is deboning to the beam.

The second type presents a substantial augmentation in the applied load; of about 90%, 104%, and 127% in beams 2B-1C-D10, 4B-H-1C-D10, 4B-V-1C-D10, 2B-2C-D10 and 2B-3C-D10, respectively. Afterward, the load suddenly decreases until it reaches about 12–20 KN. This is because the GFRP sheet separates from the beam in the middle. Then, it goes back to increase until it arrives at 22.5 kN, 30 kN, 35 kN, 40 kN, and 50 kN for beams 2B-1C, 4B-H-1C, 4B-V-1C, 2B-2C, 2B-3C, respectively. Finally, main flexural cracks occur with a significant deflection increase until failure. This flexibility is because of the development of the pressure diameter around the bolts. The pressure is controlled by three factors the GFRP thickness, the number, and the position of the bolts.

Nevertheless, with a change in diameter, the behavior changes slightly. After a sudden decrease in the applied load, it returns to rise again. The sharp reduction is noticed due to the instantaneous debonding in the pure bending section. Since the interface remained wellbonded to the end-anchor plate, the beam kept supporting the applied load. As it is further increases, the GFRP plate completely fails. The load shows a rapid fall like 4B-2C-D6, 8B-3C-D6, or a slowing down of the load with a substantial deflection rise like 4B-1C-D6, 8B-1C-D6, 8B-2C-D6. Because of the presence of the end anchor, the sample can continue to support the load.

Finally, the third type is presented with two peaks; the first peak of the load is about 98%, 166%, and 188% in beams 4B-V-2C, 4B-H-2C, 4B-V-3C, 4B-H-3C, 8B-1C, 8B-1C, 8B-2C, 8B-3C, respectively. The applied load increases again until the second peak due to the strength of the end-anchorage system. Then, the next sudden drop appears as the samples cannot allow the additional load. This sudden decrease is due to failure in the left or right part of the beam outside the reinforced area.

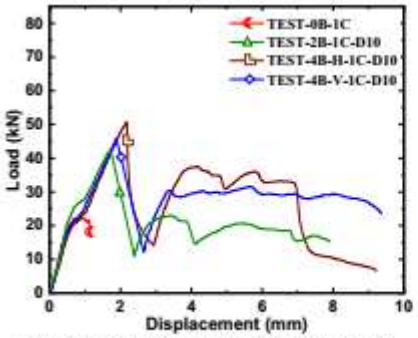

(a) Without using end anchorage GFRP

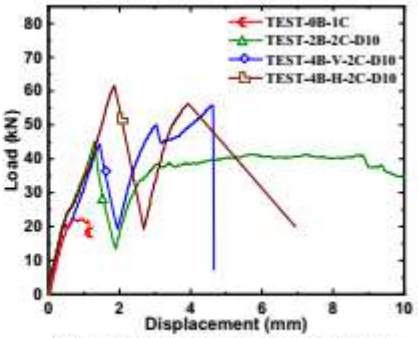

(b) End anchorage GFRP of 2.4 mm thickness

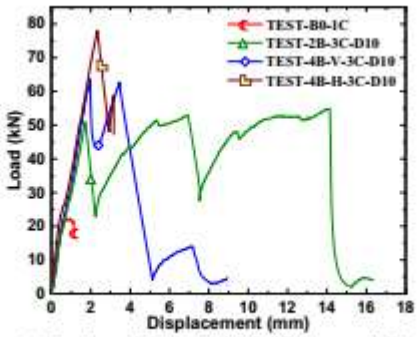

(c) End-anchorage GFRP of 4.8 mm thickness

Fig. 4 Typical load versus mid-span deflection curves with variation in position of bolts

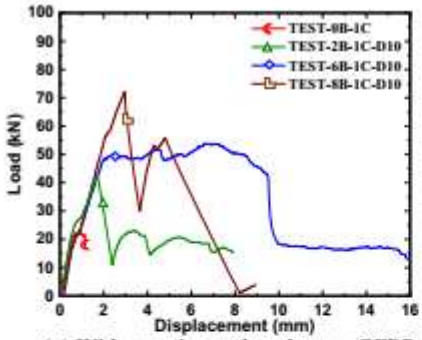

(a) Without using end-anchorage GFRP

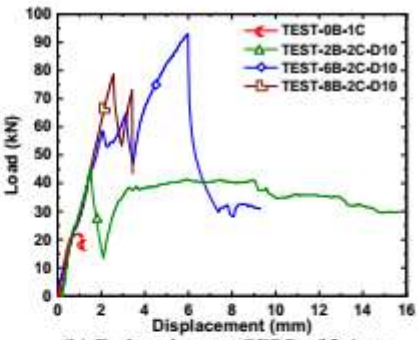

(b) End anchorage GFRP of 2.4 mm thickness

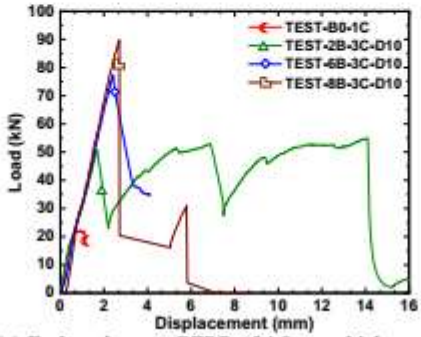

(c) End-anchora e GFRP of 4.8 mm thickness

Fig. 5 Typical load versus mid-span deflection curves with variation in number of bolts

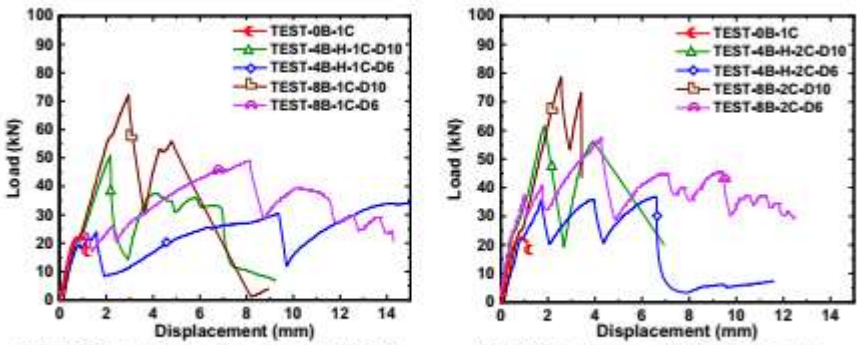

(a) Without using end-anchorage GFRP

(b) End-anchorage GFRP of 2.4 mm thickness

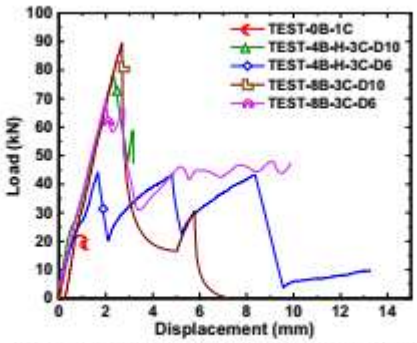

(c) End-anchorage GFRP of 4.8 mm thickness

Fig. 6 Typical load versus mid-span deflection curves with variation in diameter of bolt

3.2 Failure Mode and Cracking Pattern

Figs. 7 and 8 display pictures of below-reinforced beams strengthened with bolts-end anchoring GFRP composites (BEGFRPC) systems after failure. Different local and global failure modes include concrete cracks, crushing of GFRP plate, flexural damage, and shear cracks. The beam strengthened by bolts-end anchoring GFRP systems observed the debonding and delamination.

While under load, a sudden crack formed in the middle of the beam, which expanded rapidly with rising load until the glass FRP sheet debonded from one side of the notch. Fig. 7a shows the failure mode of the control beam (0B-1C); the flexural crack is developed at the mid-span in the maximum moment region. The maximum load capacity of this beam is about 23 kN, corresponding to a displacement of 0.5 mm.

Figs. 7 and 8 display the failure modes for beams strengthened with bolts. The bolts' numbers, positions, and diameters have been investigated in this test. As displayed in Figs. 7b and 8a, the strengthened beams 2B-1C-D10, 4B-H-1C-D10, 4B-V-1C-D10, 6B-V-1C-D10, 4B-H-1C-D6, flexural cracks are initially formed in the maximum moment region and simultaneously anchoring plates remain attached to the bolts. This attachment allows the beams to resist new loads. With an increase in the applied load, a great diameter pressure on the bolts is developed, which leads to crashing in the GFRP plate after the second peak load. As a result, the load capacity decreases, and deflection increases until the typical ductile flexural failure mode takes place. However, for beams 8B-1C-D10 and 8B-1C-D6, occurs near the last bolts leading to a shear failure mode.

The main failure modes in all BEGFRP beams of 2.4 and 4.8 mm thickness are initially flexural cracks at the mid-span. Then, the debonding occurs near the last bolts leading to a shear failure regardless of the position and diameter of the bolts. In addition, the shear cracks always occur near the supports In addition, the shear cracks always occur near the supports, and then they propagate in different directions. For example: for a beam with a GFRP thickness of 2.4 mm and the number of bolts 2 or 4, the degree of inclination is greater than 60°, but for eight bolts, it is less than 60°. As for a beam with a GFRP thickness of 4.8 mm, the crack inclination angle for two bolts is greater than 60 degrees, but in the other cases, it is much less. In addition, Figs. 7b–d and 8 show that beams strengthened with different bolts (in number, position, and diameter) do not have the same capacity and shape of failure. However, the interaction between the concrete and the glass FRP is reasonable due to the use of bolts.

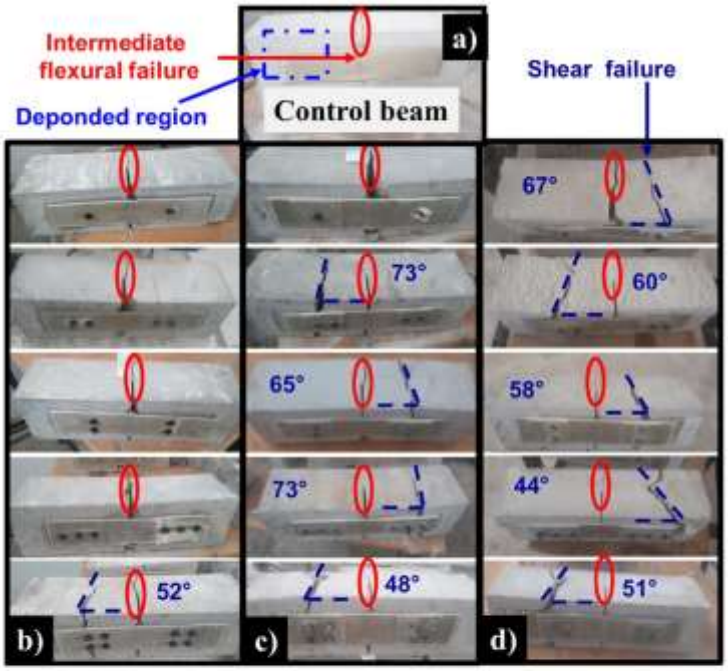

Fig. 7 Typical failure modes for beams strengthened with bolt (diameter 10 mm)-glass fiber polymer composites (BGFPC) systems: **a** control beam; **b** without using end-anchorage GFRP; **c** end anchorage GFRP of 2.4 mm thickness; **d** end-anchorage GFRP of 4.8 mm thickness

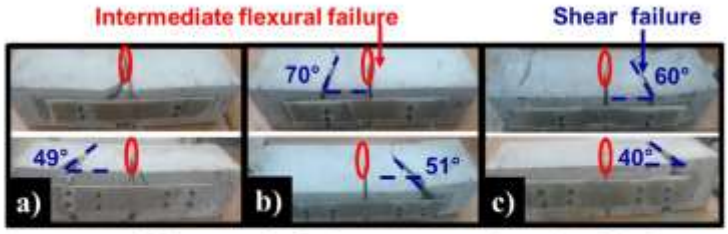

Fig. 8 Typical failure modes for beams strengthened with bolt (Diameter 6 mm)-glass fiber polymer composites (BGFPC) systems: **a** without using end-anchorage GFRP; **b** end-anchorage GFRP of 2.4 mm thickness; **c** end-anchorage GFRP of 4.8 mm thickness

3.3 Elastic Stiffness

Based on the previous load–deflection curves, Fig. 9a, b shows the values of the elastic stiffness (KE) obtained by evaluating the slope before the first appearance of the main flexural crack. For easy comparison, the elastic stiffness of the below-reinforced beams strengthened with bolt-glass fiber polymer composites (BGFPC) is normalized against the control beam. It is noticed that without end-anchorage GFRP, the elastic stiffness is not improved, whatever the bolts quantity used. Furthermore, the influence of the thickness of end-anchorage GFRP on elastic stiffness (KE) is relatively limited. For example, the enhancement in (KE) when using four horizontal bolts is 1.3 (30%) and 1.27 (27%) for end-anchorage GFRP thickness of 2.4 mm and 4.8 mm, respectively. However, these percentages are, respectively, 44% and 41% more than that obtained without end-anchorage GFRP. Therefore, end-anchorage GFRP is too necessary for such reinforcement. The optimal thickness of the endanchorage GFRP will be determined after analyzing figures related to the ultimate flexural load and the energy absorption.

The effect of bolt diameter and end-anchorage thickness on the normalized elastic stiffness of the beams strengthened with (BGFPC) is shown in Fig. 10a, b using 4 and 8 bolts, respectively. As can be seen, added glass fiber polymer composites with intermediate and high thickness cause an increase in the elastic stiffness of the beams. In addition, bolts of 10 mm in diameter are mainly sufficient to obtain relatively high elastic stiffness. The values of the elastic stiffness obtained from the load–deflection relationship are given in Table 4.

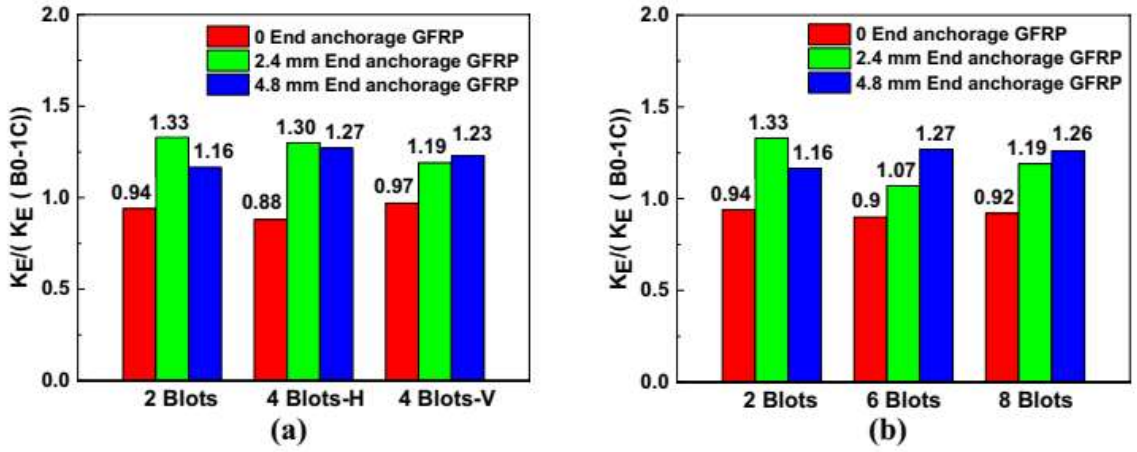

Fig. 9 Normalized elastic stiffness versus bolt quatity (diameter 10 mm) and end-anchorage thickness

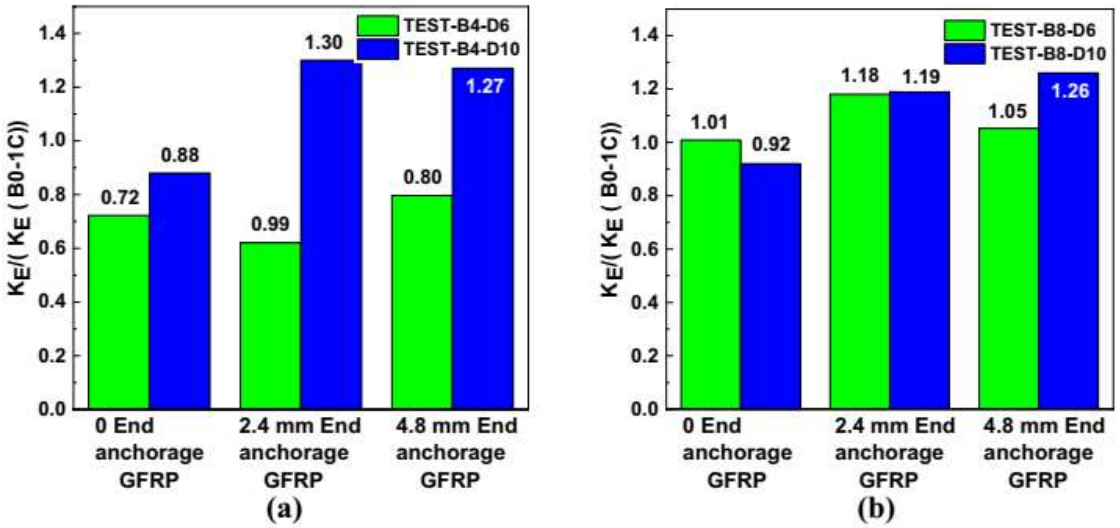

Fig. 10 Normalized elastic stiffness versus bolt diameter and end anchorage thickness

3.4 Ultimate Loads and Flexural Capacity

Fig. 11a, b provides the ultimate loads of the below-reinforced beams strengthened with (BGFPC). In general, the force that creates failure in the beam is increased by increasing the bolt quantity and the thickness of the anchorage GFRP. Six bolts with a GFRP of 2.4 mm are mainly sufficient to obtain relatively high ultimate loads. In addition, in the case of using four horizontal bolts, it is necessary to increase the thickness of the anchorage GFRP to 4.8 mm.

Figs. 11a and b provide the ultimate loads of the belowreinforced beams strengthened with (BGFPC) using 4 and 6–8 bolts, respectively.

Figs. 12a and b shows the effect of bolt diameter and end-anchorage thickness on the normalized ultimate load of the strengthened beams using 4 and 8 bolts, respectively. It is noticed that the bolts of 10 mm in diameter give a high ultimate load, whatever their quantity.

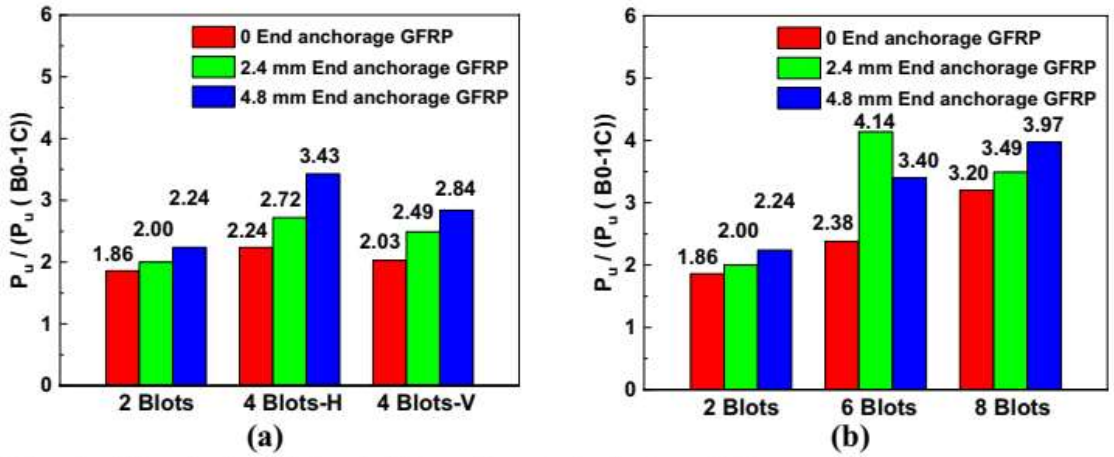

Fig. 11 Normalized ultimate load versus bolt quatity (diameter 10 mm) and end-anchorage thickness

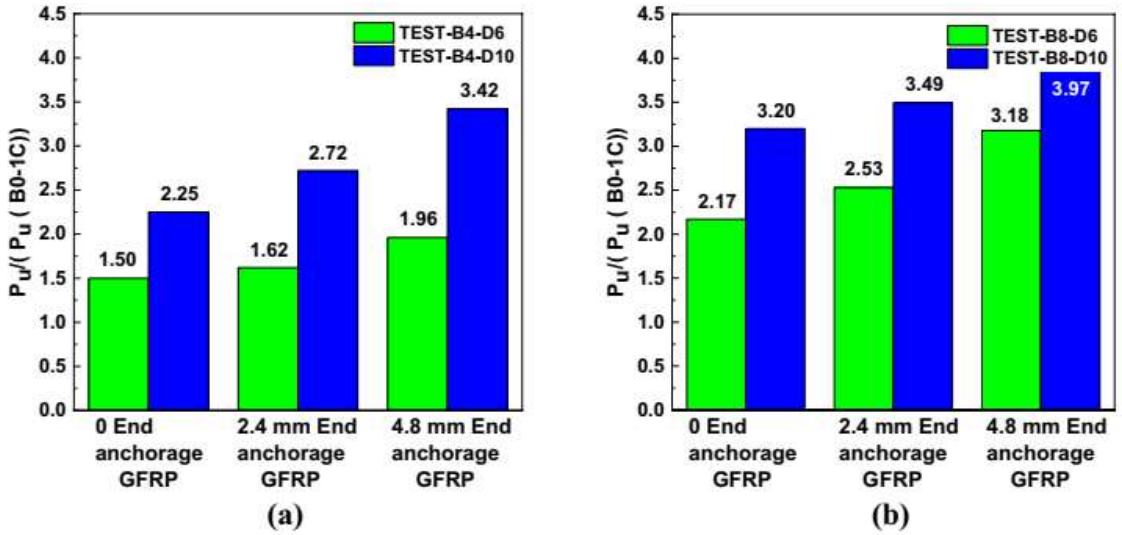

Fig. 12 Normalized ultimate load versus bolt diameter and end-anchorage thickness

4. Conclusions

mainly sufficient to obtain relatively high ultimate loads. In addition, in the case of using four horizontal bolts, it is necessary to increase the thickness of the anchorage GFRP to 4.8 mm. Figs. 11a and b provide the ultimate loads of the belowreinforced beams strengthened with (BGFPC) using 4 and 6–8 bolts, respectively. Figs. 12a and b shows the effect of bolt diameter and end-anchorage thickness on the normalized ultimate load of the strengthened beams using 4 and 8 bolts, respectively. It is noticed that the bolts of 10 mm in diameter give a high ultimate load, whatever their quantity. The values of the ultimate load obtained from the loaddeflection relationship are shown in Table 4. 4B-V-3C, 4B-H-3C, 8B-1C, 8B-1C, 8B-2C, 8B-3C, respectively. The next sudden drop appears as the beams cannot allow the additional load. This sudden decrease is due to failure in the left or right part of the beam outside the reinforced area. On the other hand, the beams strengthened with six bolts and end-anchorage GFRP of 2.4 mm thickness had shown a significant deformation before failure, higher energy absorption capacity with lower stiffness than control beams. In addition, such beams have the most increased shear crack angle, 73°. This orientation confirmed that the bolts tend to be involved in the reinforcement mechanism. The present findings will be adopted in numerical simulations of time-consuming experiments of RC structures subjected to bending loading.

Acknowledgements

This research did not receive any specific grant from funding agencies in the public, commercial, or not-for-profit sectors.

Conflict of Interests

The Author(s) declare(s) that there is no conflict of interest.

References

A.C. Institute. (2008). Guide for the design and construction of externally bonded FRP systems for strengthening concrete structures, In ACI 440.2 R-08, American Concrete Institute.

ACI 211.1–Reapproaved 2009. (2009). Standard practice for selecting proportions for normal, heavyweight, and mass concrete, An ACI Standard Reported by ACI Committee 211 (p. 38).

Alasadi, S., Ibrahim, Z., Shafigh, P., Javanmardi, A., & Nouri, K. (2019). An experimental and numerical study on the flexural performance of overreinforced concrete beam strengthening with bolted-compression steel plates: Part II. Applied Sciences, 10(1), 94. https://doi.org/10.3390/app10 010094

Al-Hamrani, A., & Alnahhal, W. (2021). Shear behavior of basalt FRC beams reinforced with basalt FRP bars and glass FRP stirrups: Experimental and analytical investigations. Engineering Structures, 242, 112612. https://doi. org/10.1016/j.engstruct.2021.112612

Ali, H. M., Sheikh, M. N., & Hadi, M. N. (2022). Flexural strengthening of RC beams with NSM-GFRP technique incorporating innovative anchoring system. Structures, 38, 251–264. https://doi.org/10.1016/j.istruc.2022.01. 088

AminiPishro, A., Zhang, S., Zhang, Z., Zhao, Y., AminiPishro, M., Zhang, L., & Postel, V. (2022a). Structural behavior of FRP-retrofitted RC beams under combined torsion and bending. Materials, 15(9), 3213. https://doi.org/10. 3390/ma15093213

AminiPishro, A., Zhang, Z., AminiPishro, M., Liu, W., Zhang, L., & Yang, Q. (2022b). Structural performance of EB-FRP-strengthened RC T-beams subjected to combined torsion and shear using ANN. Materials, 15(14), 4852. https:// doi.org/10.3390/ma15144852

ASTM. (2010). D638–10 Standard test method for tensile properties of plastics. American Society for Testing and Materials.

ASTM. (2017). Standard test method for evaluation of performance for FRP composite bonded to concrete substrate using beam test; ASTM D7958/D7958M. ASTM.

ASTM C39/C39M-17b. (2017). Standard test method for compressive strength of cylindrical concrete specimens. ASTM International.

Chen, C., Cheng, L., Sui, L., Xing, F., Li, D., & Zhou, Y. (2018a). Design method of end anchored FRP strengthened concrete structures. Engineering Structures, 176, 143–158. https://doi.org/10.1016/j.engstruct.2018.08.081

Chen, W., Pham, T. M., Sichembe, H., Chen, L., & Hao, H. (2018b). Experimental study of flexural behaviour of RC beams strengthened by longitudinal and U-shaped basalt FRP sheet. Composites Part B Engineering, 134, 114–126. https://doi.org/10.1016/j.compositesb.2017.09.053

Del Rey Castillo, E., Griffith, M., & Ingham, J. (2018). Seismic behavior of RC columns flexurally strengthened with FRP sheets and FRP anchors. Composite Structures, 203, 382–395. https://doi.org/10.1016/j.compstruct. 2018.07.029

Djeddi, F., Ghernouti, Y., Abdelaziz, Y., & Alex, L. (2016). Strengthening in flexure–shear of RC beams with hybrid FRP systems: Experiments and numerical modeling. Journal of Reinforced Plastics and Composites, 35(22), 1642–1660. https://doi.org/10.1177/0731684416662532

El Ghadioui, R., Wagner, J., Klein, J., Proske, T., Curbach, M., & Graubner, C. A. (2022). RC members with a flexural-strengthening layer of CFRP textilereinforced concrete under monotonic and cyclic long-term loading. Structural Concrete, 23(2), 939–953. https://doi.org/10.1002/suco.20210 0452

Esmaeili, J., Aghdam, O. R., Andalibi, K., Kasaei, J., & Gencel, O. (2022). Experimental and numerical investigations on a novel plate anchorage system to solve FRP debonding problem in the strengthened RC beams. Journal of Building Engineering, 45, 103413. https://doi.org/10.1016/j.jobe.2021. 103413

Garhwal, S., Sharma, S., & Sharma, S. K. (2021). Monitoring the flexural performance of GFRP repaired corroded reinforced concrete beams using passive acoustic emission technique. Structural Concrete, 22(1), 198–214. https://doi.org/10.1002/suco.202000247

Mhanna, H. H., Hawileh, R. A., & Abdalla, J. A. (2021, December). Effect of FRP Anchor Inclination Angle on Shear Strengthening of Reinforced Concrete T-beams. In International Conference on Fibre-Reinforced Polymer (FRP) Composites in Civil Engineering (pp. 2169–2179). Springer. https://doi. org/10.1007/978-3-030-88166-5_187

Nguyen, H., Mutsuyoshi, H., & Zatar, W. (2015). Hybrid FRP-UHPFRC composite girders: Part 1–experimental and numerical approach. Composite Structures, 125, 631–652. https://doi.org/10.1016/j.compstruct.2014.10.038

Nili, M., Sasanipour, H., & Aslani, F. (2019). The effect of fine and coarse recycled aggregates on fresh and mechanical properties of self-compacting concrete. Materials, 12(7), 1120. https://doi.org/10.3390/ma12071120

NoroozOlyaee, M., & Mostofinejad, D. (2019). Slenderness effects in circular RC columns strengthened with CFRP sheets using different external bonding techniques. Journal of Composites for Construction, 23(1), 04018068. https://doi.org/10.1061/(ASCE)CC.1943-5614.0000908

Pavithra, C., Revathy, J., & Gajalakshmi, P. (2022). Structural behavior of hybrid double-skin tubular FRP–concrete–steel column: State-of-the-art review. Innovative Infrastructure Solutions, 7(1), 1–19. https://doi.org/10.1007/ s41062-021-00653-3

Pishro, A. A., & Feng, X. (2017). RC beams behavior retrofitted by FRP subjected to torsion, shear and flexure-a review. International Journal of Computer Science and Network Security (IJCSNS), 17(2), 34.

Salama, A. S. D., Hawileh, R. A., & Abdalla, J. A. (2019). Performance of externally strengthened RC beams with side-bonded CFRP sheets. Composite Structures, 212, 281–290. https://doi.org/10.1016/j.compstruct.2019.01.045

Sankaramoorthy, T., Karthikeyan, R., Pradeep, G. M., Athikesavan, D., & Girimurugan, R. (2022). Improved performance of confinement of RC beam with glass fibre reinforced polymer laminates. Materials Today: Proceedings, 56, 3190–3195. https://doi.org/10.1016/j.matpr.2021.09.280

Sharma, G., Sharma, S., & Sharma, S. K. (2022). Monitoring structural behaviour of concrete beams reinforced with steel and GFRP bars using acoustic emission and digital image correlation techniques. Structure and Infrastructure Engineering, 18(2), 167–182. https://doi.org/10.1080/15732479. 2020.1836661

Tran, Q. D., Nhut, P. V., & Matsumoto, Y. (2022). Multi-bolted connection for pultruded glass fiber reinforced polymer's structure: A study on strengthening by multiaxial glass fiber sheets. Polymers, 14(8), 1561. https://doi.org/ 10.3390/polym14081561

Tudjono, S., Lie, H. A., & Hidayat, B. A. (2015). An experimental study to the influence of fiber reinforced polymer (FRP) confinement on beams subjected to bending and shear. Procedia Engineering, 125, 1070–1075.
https://doi.org/10.1016/j.proeng.2015.11.164

Vahidpour, M., Kheyroddin, A., & Kioumarsi, M. (2022). Experimental investigation on flexural capacity of reinforced concrete beams strengthened with 3D-fiberglass, CFRP and GFRP. International Journal of Concrete Structures and Materials, 16(1), 1–20. https://doi.org/10.1186/s40069-022-00508-w

Yahiaoui, D., Saadi, M., & Bouzid, T. (2022). Compressive behavior of concrete containing glass fibers and confined with glass FRP composites. The International Journal of Concrete Structures and Materials, 16(1), 1–19. https:// doi.org/10.1186/s40069-022-00525-9

Zhang, S. S., Ke, Y., Smith, S. T., Zhu, H. P., & Wang, Z. L. (2021). Effect of FRP U-jackets on the behaviour of RC beams strengthened in flexure with NSM CFRP strips. Composite Structures, 256, 113095. https://doi.org/10.1016/j.compstruct.2020.113095

Zhou, Y., Chen, X., Fan, Z., Sui, L., Li, D., & Xing, F. (2017). Bond behaviors of FRP-to-concrete interface under the control of a novel end-anchorage system. Composite Structures, 168, 130–142. https://doi.org/10.1016/j.compstruct.2017.02.056

Zhou, Y., Wang, X., Sui, L., Xing, F., Wu, Y., & Chen, C. (2018). Flexural performance of FRP-plated RC beams using H-type end anchorage. Composite Structures, 206, 11–21. https://doi.org/10.1016/j.compstruct.2018.08.015